GEOPHYSICS, VOL. 72, NO. 1 (JANUARY-FEBRUARY 2007); P. E15–E25, 9 FIGS., 1 TABLE.
10.1190/1.2364849

Seismic velocities of unconsolidated sands: Part 2 — Influence of sorting- and compaction-induced porosity variation

Michael A. Zimmer[1], Manika Prasad[2], Gary Mavko[3], and Amos Nur[3]

ABSTRACT

Unaccounted-for porosity variation in unconsolidated sediments can cloud the interpretation of the sediment's seismic velocities for factors such as fluid content and pressure. However, an understanding of the effects of porosity variation on the velocities can permit the remote characterization of porosity with seismic methods. We present the results of a series of measurements designed to isolate the effects of sorting- and compaction-induced porosity variation on the seismic velocities and their pressure dependences in clean, unconsolidated sands. We prepared a set of texturally similar sand and glass-bead samples with controlled grain-size distributions to cover an initial porosity range from 0.26 to 0.44. We measured the compressional- and shear-wave velocities and porosity of dry samples over a series of hydrostatic pressure cycles from 0.1 to 20 MPa. Over this range of porosities, the velocities of the dry samples at a given pressure vary by $<15\%$. However, the water-saturated compressional-wave velocities, modeled with Gassmann fluid substitution, demonstrate a consistent increase with decreasing porosity. In both the dry and water-saturated cases, the porosity trend at a given pressure is approximately described by the isostress (harmonic) average between the moduli of the highest-porosity sample at that pressure and the moduli of quartz, the predominant mineral component of the samples. Empirical power-law fit coefficients describing the pressure dependences of the dry bulk, shear, and constrained (P-wave) moduli from each sample also demonstrate no significant, systematic relationship with the porosity. The porosity dependence of the water-saturated bulk and constrained moduli is primarily contained in the empirical coefficient representing the modulus at zero pressure.

INTRODUCTION

High-resolution seismic techniques are increasingly being used to image unconsolidated sediments in shallow aquifers and at potential offshore drill sites. When suitably collected, these high-resolution data can be used to characterize sediment properties with technologies previously developed to characterize consolidated reservoir rocks such as impedance inversion and AVO analysis. The characterization of unconsolidated sands is of particular interest as the sands make up the permeable part of the shallow sedimentary column and are especially prone to failure, resulting in shallow-water flows and sand production. The flow and mechanical properties of clean sands are primarily controlled by their porosity and by the effective pressure. The remote characterization of these properties therefore requires the development of empirical or theoretical relationships among the porosity, effective pressure, and seismic velocities, as have been developed for more consolidated clastic rocks (Wyllie et al., 1958; Han et al., 1986; Walton, 1987; Eberhart-Phillips et al., 1989; Freund, 1992; Jones, 1995; Khaksar et al., 1999).

Two of the key controls on the porosity in unconsolidated sands are sorting and compaction. Better sorting, or a narrower particle-size distribution, generally results in a higher porosity (Beard and Weyl, 1973; Cumberland and Crawford, 1987). In poorly sorted sand, many of the smaller grains can fit within the open pores so that there is only minimal expansion of the matrix of larger grains, thereby reducing the porosity. Likewise, the larger the stresses that a sand

Manuscript received by the Editor March 4, 2006; revised manuscript received May 27, 2006; published online December 20, 2006; corrected version published online December 21, 2006.
[1]Formerly Stanford University, Stanford, California; presently ENSCO, Inc., 5400 Port Royal Road, Springfield, Virginia 22151. E-mail: zimmer.michael@ensco.com.
[2]Colorado School of Mines, Department of Geophysics, 1500 Illinois Street, Golden, Colorado 80401. E-mail: mprasad@mines.edu.
[3]Stanford University, Department of Geophysics, Rock Physics Laboratory, 397 Panama Mall, Stanford, California 94305. E-mail: mavko@stanford.edu; anur@stanford.edu.

has been exposed to, the greater the compaction that it will have undergone and the lower its porosity will be.

In this study, we have sought to measure the effects of porosity variation that result from sorting and compaction on the seismic velocities. We sought to observe the effects of these porosity changes both on the velocities at a given pressure and on their pressure dependences over pressures from 0.1 to 20 MPa. To isolate the effects of porosity variation specifically caused by sorting and compaction, we prepared a set of synthetic sand and glass-bead samples with controlled grain-size distributions to cover a range of initial porosities from 0.26 to 0.44. We then measured the compressional- and shear-wave velocities of these samples over hydrostatic pressure cycles from 0.1 to 20 MPa. We compare these laboratory results to the velocity versus porosity trends observed in previous measurements on unconsolidated sands. The direct velocity versus pressure relationships observed in the data presented in this paper are discussed in Zimmer et al. (2007).

Existing velocity-porosity trends in unconsolidated sands

For the low pressures (<0.7 MPa) typical of most geotechnical applications, Hardin and Blandford (1989) developed a widely accepted empirical relationship relating the effective pressure, porosity, and shear or constrained (P-wave) modulus of unconsolidated sediments. Their relationship is given for an isotropic stress state as follows:

$$M_{ij} = \frac{\mathrm{OCR}^k}{F(e)} \frac{S_{ij}}{F(\nu)} p_a^{1-n} p'^n. \quad (1)$$

Here M_{ij} is the modulus of interest, p' is the effective stress, p_a is the atmospheric pressure, $F(\nu)$ is a function of the Poisson's ratio of the grain material and differs depending on the modulus being fit, and S_{ij} and n are free parameters. The overconsolidation ratio (OCR) is defined as the preconsolidation pressure divided by the current effective pressure. The OCR term corrects for the effects of compaction on the pressure-modulus relationship, where k is a function of the plasticity index, usually assumed to be zero for sands (Hardin and Drnevich, 1972). The void-ratio function, $F(e) = 0.3 + 0.7e^2$, corrects for the effects of any porosity variation on the moduli at a given pressure. The void ratio e is deterministically related to the porosity ϕ according to $e = \phi/(1 - \phi)$. This correction was developed from shear-modulus data for a wide variety of sediment textures over a wide range of porosities. The suitability of the void-ratio function to correct the bulk or constrained modulus for the effects of porosity variation has not been tested.

On the basis of laboratory measurements at higher pressures, Blangy et al. (1993) recognized that the moduli-porosity trend of a set of texturally similar, poorly consolidated, dry sands (porosities of 0.22-0.38) could be approximated by the harmonic average between the moduli of the principal mineral and the moduli of the pore-filling clay and fluid. Using the same data set, Dvorkin and Nur (1996) found that the trend could be described by the modified Hashin-Shtrikman lower bound, averaging the principal mineral moduli and the moduli predicted by Hertz-Mindlin contact models at the critical porosity. Avseth et al. (2000) observed a similar relationship between the log-derived compressional-wave velocities and the porosities of poorly consolidated reservoir sands from the North Sea. They attributed the porosity variation to differences in sorting interpreted from particle-size distributions garnered from thin-section analysis.

EXPERIMENTAL METHODS AND SAMPLES

We collected seismic velocity data from a total of 11 synthetic samples, with initial porosities from 0.26 to 0.44 (Table 1). Four of the samples consisted of sand, and seven consisted of glass beads. The glass-bead samples were prepared to represent sediments with different degrees of sorting, while removing any effects that might result from differences in grain shape associated with variations in grain size. We prepared three single-sieve-size glass-bead samples, representing very well sorted sediments: one with a large grain size (GB Big, 0.295–0.350 mm) and two with grain sizes that were four and eight times smaller (GB Small, 0.074–0.088 mm, and GB iny, 0.037–0.044 mm). To generate samples with lower porosities, representative of more poorly sorted sediments, we also prepared three glass-bead samples (GB 35% small, GB 35% tiny 1, and GB 35% tiny 2) from a mixture of 35% (by mass) of the smaller grain sizes

Table 1. Sample summary.

	Sample name	Initial porosity	Clean, quartz sand; well sorted D_{10} = 0.178 mm, D_{60} = 0.304 mm[a]			
			Fraction	Diameter (μm)	Fraction	Diameter (μm)
Sands	Santa Cruz 1	0.414				
	Santa Cruz 2	0.438				
	SC big	0.409	1	295–350	—	—
	SC 35% small	0.380	0.65	295–350	0.35	53–88
Glass beads	GB big	0.381	1	295–350	—	—
	GB small	0.411	1	74–88	—	—
	GB 35% small	0.321	0.65	295–350	0.35	74–88
	GB tiny	0.422	1	37–44	—	—
	GB 35% tiny 1	0.296	0.65	295–350	0.35	37–44
	GB 35% tiny 2	0.258	0.65	295–350	0.35	37–44
	GB broad	0.338	1	37–710	—	—

[a] D_{10} and D_{60} are the grain diameters below which 10% or 60%, respectively, of the mass of the sample is found.

(i.e., GB small and GB tiny) and 65% of the larger grain size (i.e., GB big). A bimodal mixture of grain sizes in which the proportion of smaller grains is 35% should demonstrate the greatest decrease in porosity relative to the single-grain-size samples (Cumberland and Crawford, 1987). Similarly, two synthetic sand samples were prepared from sieve fractions of a fine-grained, well-sorted, quartz sand [Santa Cruz (SC) aggregate]. One sample (SC big) was made up of the same large grain size as the large-grained glass-bead sample (0.295–0.350 mm). A second sample (SC 35% small) was made up of 65% (by mass) of the large size fraction and 35% of 0.053–0.088 -mm-diameter grains. In addition, one glass-bead sample (GB broad) was made up of a broad, log-normal distribution of particle sizes, and two sand samples (Santa Cruz 1, Santa Cruz 2) were prepared of the full, unsieved Santa Cruz aggregate.

Each sample, 3.81 cm in diameter and 3–5 cm in length, was prepared in an instrumented sample holder built to fit within a hydrostatic-pressure vessel. Special attention was given to preparing the samples in as similar a manner as possible, while endeavoring to ensure complete mixing of the different grain sizes. However, the sample preparation differed depending on whether the sample was a single grain size or was a mixture of grain sizes. The single-size samples were air pluviated into the sample holder in a single section, whereas most of the mixed-size samples were mixed dry, split into four sections, and each section pluviated into the sample holder separately. In an attempt to produce a more homogeneous mixture, two of the samples (GB 35% tiny 2 and GB broad) were mixed after being moistened with a few milliliters of water; the mixtures were then tamped down in the sample holder and allowed to dry before being run.

Each sample was held between the two cylindrical end caps of the sample holder and was jacketed with Tygon tubing. The end caps each contain compressional and shear ultrasonic transducers, made with 200-kHz piezoelectric (PZT) crystals and with plastic faceplates (30% glass-filled polycarbonate) to improve the amount of energy transmitted through the samples. The end caps are supported by a steel frame that maintains the alignment of the transducers (within 1°) while allowing one end cap to slide freely, permitting the sample to compact and rebound with loading and unloading. The sample dimensions were determined initially by measuring the diameter of the jacket around the sample and the distance between the two end caps once the sample had been prepared in the holder. Changes in the sample volume with loading were monitored by measuring changes in the length and circumference of the samples with three linear strain gauges attached between the end caps and a circumferential gauge located around the middle of the sample. The density of the samples was calculated from the dry-sample mass and the sample volume. The porosity was calculated from the dry-sample mass, sample volume, and grain density. An error analysis of the density and porosity measurements shows the error of each to be $<3\%$.

Velocities were calculated by picking first arrivals from pulse-transmission signals. Detailed error analysis incorporating uncertainties in the initial lengths and length changes of the samples, as well as ambiguities in the arrival times picked from each individual waveform, predicts uncertainties in the velocities to be generally less than 2% for the compressional waves and 4% for the shear waves.

Each sample was loaded hydrostatically through between 1 and 9 pressure cycles with subsequently increasing peak pressures up to 20 MPa. Measurements were made at several pressures on both the loading and unloading paths of each cycle. For each pressure step, the pressure was adjusted to the desired pressure and then held constant for at least 20 min until both the strain and the ultrasonic signals stabilized before making the measurements. The larger pressure cycles, involving on the order of 20 pressure steps, commonly required a day or more to complete. The shear- and compressional-wave velocities and the porosity were measured at the same set of pressures during each cycle to allow their comparison at various levels of compaction. All of the data presented here were collected on dry samples. More detailed descriptions of the experimental apparatus and procedures can be found in Zimmer (2003).

OBSERVED POROSITY TRENDS

The initial porosities of the samples vary from 0.26 to 0.44; however, those of the sand samples are limited to a range from 0.38 to 0.44. The porosities of the glass-bead samples cover the entire porosity range. Prior to loading, the porosity variation from sample to sample results from their different grain-size distributions and particle shapes (sands versus glass beads), as well as from the different packing produced by variations in sample preparation. Besides deliberate differences in the preparation methodology, the reconstitution of identical loose samples inherently results in inadvertent variability in sample packing. For either the sands or glass beads, the grain shapes and the sample-preparation procedures were similar enough that the primary control on the initial porosity should be the grain-size distribution, or sorting. The porosity of individual samples also decreases with loading and then only partially rebounds upon unloading, as shown in Figure 1 for sample SC 35% small. In this section, we describe the effects of this sorting- and compaction-induced porosity variation on the measured velocities and their pressure dependences.

Effect of sorting-induced porosity variation on the velocities

Figure 2 shows the velocities from all 11 samples plotted against the porosity. This figure illustrates that although the different parti-

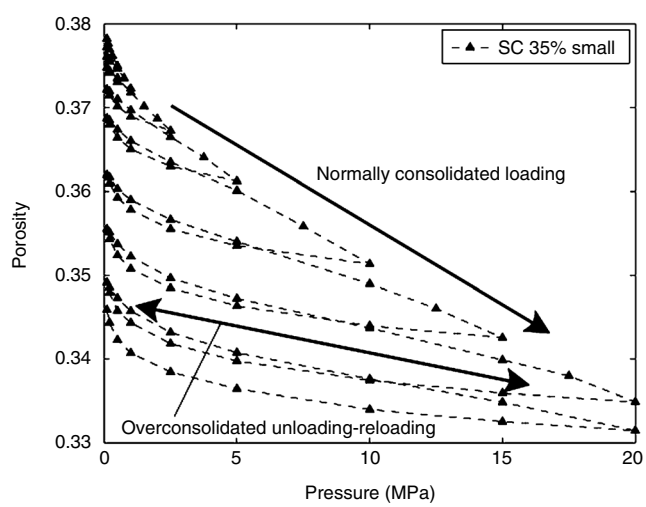

Figure 1. Porosity data for a typical sand sample, SC 35% small, loaded through a series of nine cycles with increasing peak pressures.

cle-size distributions produce a broad range of porosities, the velocity range exhibited by each of the dry samples over the loading path is very similar. The lines in Figure 2 link measurements were made at the same pressure for three sets of related samples. Each individual line links measurements made under normally consolidated conditions at each of the following pressures: 0.2, 0.5, 1, 2, 5, 10, and 20 MPa. The dotted line links points from the large-grained sand (SC big) and the mixed-grain-size sand (SC 35% small). The dashed line links the measurements from the large-grained glass-bead sample (GB big), the sample that is a mix of 65% large and 35% small grains (GB 35% small), and the sample entirely made up of small grains (GB small). The solid line links points from the analogous set of samples that include samples GB big, GB 35% tiny 1 and GB tiny. Each of these three sets contains different combinations of two grain size end members with the same texture and sample preparation: a large-grain-size sample, a sample containing a mix of large and small grain sizes, and, for the glass beads, a small grain-size sample. These lines demonstrate the velocity-porosity trend for each of these sets of samples at each pressure. At low pressures, there is up to 50% variation in the velocities at a given pressure; the velocity of the large-grain sample is the highest in each set of samples. At the highest pressures, the lowest-porosity, mixed-grain-size glass-bead sample demonstrates velocities that are 5% to 20% higher than the single-grain-size samples. The two sand samples demonstrate essentially equal velocities at higher pressures.

Figure 3 shows the velocity data from all of the samples, as shown in Figure 2, but with each data point color-coded by the effective pressure at which the velocity measurement was made. This figure demonstrates that at pressures below 1 MPa, little or no systematic porosity-dependent variation is seen in either the compressional- or shear-wave velocities measured in these dry samples. Above 1 MPa, the velocities increase slightly with decreasing porosity for both velocities; increases are up to 10% for V_S and up to 15% for V_P at the highest pressures. The two samples that were prepared by moist tamping, GB 35% tiny 2 and GB broad, stand out in that their velocities at any given pressure lie below the trends observed for the other samples. Nevertheless, the other samples, even though they include both sand and glass-bead samples with various particle-size distributions, demonstrate similar velocity values and consistent velocity-porosity trends at a given pressure.

The lines superimposed on the data in Figure 3 represent the velocity-porosity trends for a given pressure modeled in three ways. The dashed lines demonstrate the trend of the empirical porosity correction developed by Hardin and Blandford (1989). The dotted and solid lines represent model trends based on modified forms of the Hashin-Shtrikman lower bound and the Reuss bound, respectively. Both are calculated from the quartz moduli and the moduli of the highest-porosity sample (Santa Cruz 2) at each pressure. Because these model trends are insensitive to the mineral end point within the porosity range of these samples, the moduli of quartz were used to represent the mineral moduli of all of the samples. The Reuss bound, the weighted harmonic average between the two end-member moduli, simulates the weakest possible way to combine two distinct materials (Mavko et al., 1998). Here the modified Reuss average demonstrates the minimum possible effect on the velocities of mixing solid grain material with the granular framework of the highest-porosity sample at a given pressure. This modified Reuss average was calculated as follows:

$$\frac{1}{M} = \frac{f_{df}}{M_{df}} + \frac{f_{\mathrm{Qtz}}}{M_{\mathrm{Qtz}}}, \tag{2}$$

where M is the resulting average modulus, M_{df} is the modulus of the dry frame at the pressure of interest, and M_{Qtz} is the modulus of pure quartz. The fraction of dry frame, f_{df}, is given by $f_{df} = \phi/\phi_0$, where ϕ is the porosity and ϕ_0 is the porosity of the highest-porosity sample (Santa Cruz 2) at that pressure. The fraction of pure quartz, f_{Qtz}, is $1 - f_{df}$, or $(1 - \phi/\phi_0)$. The high-porosity limit ϕ_0 differs from the concept of the critical porosity (Nur et al., 1995) in that ϕ_0 represents the high-porosity limit of a texturally diverse set of samples that decreases with increasing pressure, whereas the critical porosity is the high-porosity limit for a specific sediment at zero pressure.

The Hashin-Shtrikman lower bound (Hashin and Shtrikman, 1963) also expresses the theoretical lower limit of the mixture of two substances, but differs from the Reuss bound in that the former assumes an idealized mixing geometry in which the softer sand framework forms a shell around spheres of solid quartz. The bulk and

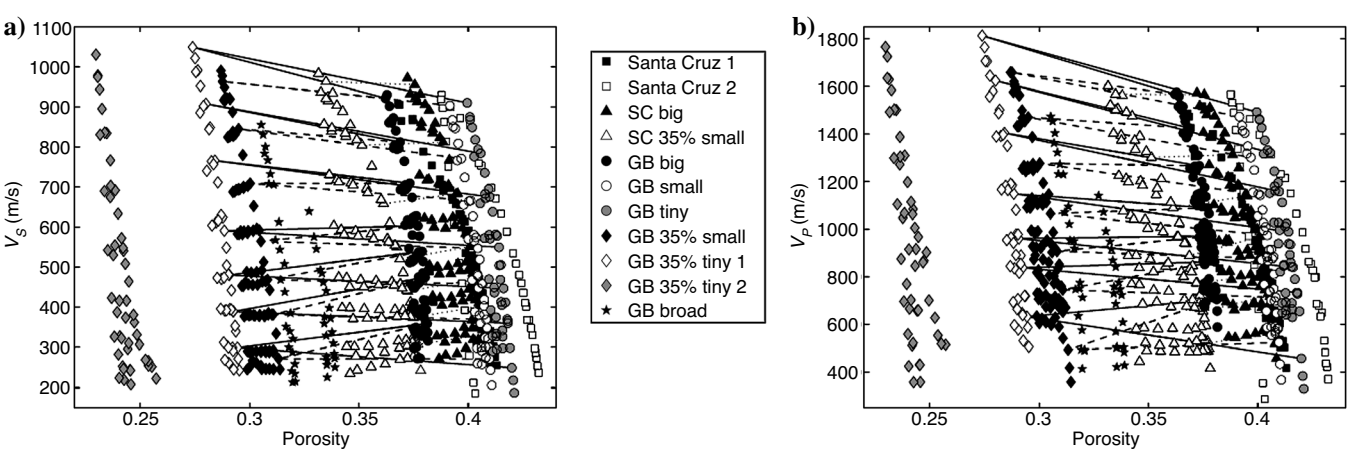

Figure 2. Velocity data measured for each dry sample at all pressures, plotted against the porosity. (a) Shear-wave velocities. (b) Compressional-wave velocities.

shear moduli of the mixture, K^{HS} and μ^{HS}, were calculated according to the following expressions:

$$K^{HS} = K_{df} + \frac{f_{Qtz}}{(K_{Qtz} - K_{df})^{-1} + f_{df}\left(K_{df} + \frac{4}{3}\mu_{df}\right)^{-1}}, \quad (3)$$

$$\mu^{HS} = \mu_{df} + \frac{f_{Qtz}}{(\mu_{Qtz} - \mu_{df})^{-1} + \frac{2f_{df}(K_{df} + 2\mu_{df})}{5\mu_{df}\left(K_{df} + \frac{4}{3}\mu_{df}\right)}}, \quad (4)$$

with the fractions of the two components calculated as for the Reuss average.

The Hardin and Blandford porosity trend was calculated by normalizing the empirically derived void-ratio function $F(e)$ of equation 1, at the current void ratio e by the value at the dry-frame void ratio e_{df}. This value was then multiplied by the high-porosity dry-frame modulus for the pressure of interest M_{df} as follows:

$$M = \frac{F(e_{df})}{F(e)} M_{df} = \frac{0.3 + 0.7e_{df}^2}{0.3 + 0.7e^2} M_{df}, \quad (5)$$

where M is the resulting porosity-corrected modulus.

Gassmann fluid substitution was used to model the water-saturated velocities from the velocities, density, and porosity measured in the dry samples. We chose to use Gassmann model predictions to evaluate the porosity dependence of the velocities rather than direct measurements on water-saturated samples because of the presence of frequency dispersion at the high frequencies of our measurement apparatus. This dispersion may produce a different porosity dependence than would be observed at the low frequencies typically used for field measurements. However, violation of the Gassmann theory's simplifying assumptions, including the assumption that the moduli of the sediment frame are not affected by fluid saturation, as well as errors in the input parameters of the model, could lead to inaccuracy in the predicted velocities. Nevertheless, we think that the Gassmann theory has been verified sufficiently to justify using these results as reasonable approximations of the porosity trends to be expected in low-frequency measurements in unconsolidated sands.

Figure 4, showing the fluid-substituted compressional-wave velocities plotted against the porosity, demonstrates that lower porosities consistently result in significantly higher compressional-wave velocities for water-saturated sands. The difference of 300 m/s (~15%) between the low- and high-porosity samples is similar in relative magnitude to that of the dry compressional-wave velocities at high pressure. However, in the water-saturated case, the trend is both very consistent at all pressures and much more significant relative to the pressure-related velocity change, which is half that observed in the dry case. The shear-wave velocities, which require only a density substitution in Gassmann's theory, demonstrate behavior very similar to the dry velocities (Figure 3a). The lines in Figure 4 also show the velocity-porosity trends predicted by the modified Hashin-Shtrikman and Reuss averages and by the Hardin and Blandford empirical correction for the water-saturated compressional-wave velocities.

Although considerable variability exists in the velocity data, likely because the data come from reconstituted samples of various textures, all three trend lines approximately describe the velocity-porosity trend observed in the dry measurements. In the dry case, both the Reuss and Hashin-Shtrikman trends predict a relatively flat velocity-porosity relationship down to a porosity of ~0.2. They then rise steeply to the velocities of the pure mineral at zero porosity: 4120 m/s for the shear waves and 6040 m/s for the compressional waves (Mavko et al., 1998). The steeper Hashin-Shtrikman trend line does tend to overpredict the velocities at the lowest porosities by up to 10% at high pressure, especially for the shear-wave velocities. For the water-saturated compressional-wave velocities, both the Reuss and Hashin-Shtrikman trends provide estimates within 5% of the Gassmann-modeled velocity-porosity trend. However, the concave-downward trend of the Hardin and Blandford correction diverges by up to 10% from the modeled velocities in the middle of the

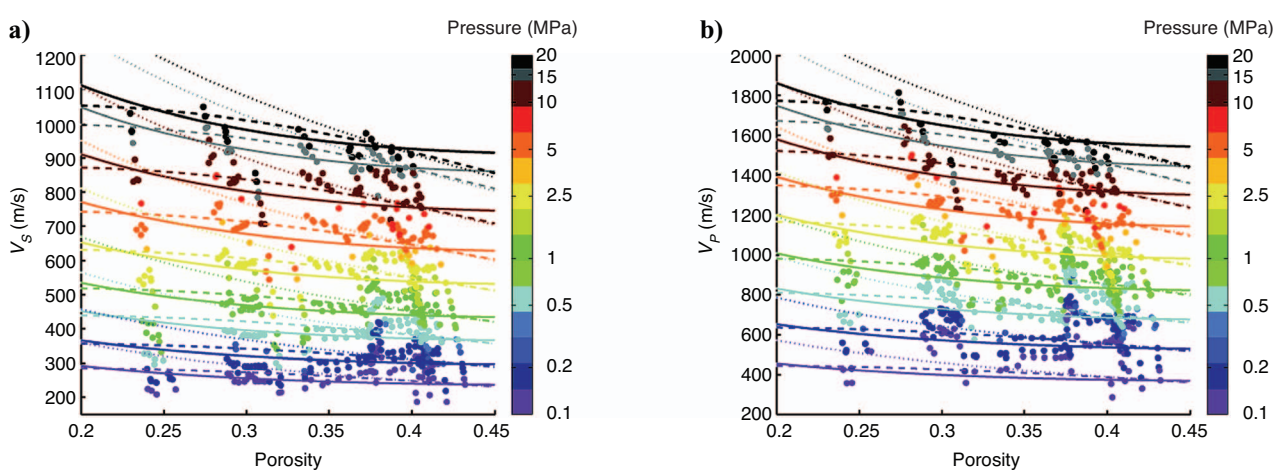

Figure 3. Velocity data from dry samples plotted against the porosity and color-coded by pressure. (a) Shear-wave velocities. (b) Compressional-wave velocities. Porosity trends: modified Reuss average (solid), modified Hashin-Shtrikman lower bound (dotted), and Hardin and Blandford empirical (dashed).

porosity range covered. The Hardin-Blandford correction would also be expected to diverge from the velocity-porosity trend again at porosities below the range tested, where this empirical correction flattens but where a continued increase in the velocities with decreased porosity would be predicted from the Gassmann theory.

Effect of compaction-induced porosity variation on the velocities

The two plots in Figure 5, showing the velocities of sample SC 35% small plotted against porosity and color-coded by the pressure, illustrate that the velocities for a given sample at a given pressure can be seen to increase slightly on preconsolidation to higher pressures. These figures demonstrate that the compaction-induced velocity-porosity trend for both the shear- and compressional-wave velocities is effectively flat at low pressures, but steepens at higher pressures. The Reuss, Hashin-Shtrikman, and Hardin-Blandford porosity-trend lines superimposed on the data, anchored at the velocity value on the initial loading path, illustrate the approximate effect of the sorting-induced porosity variation on the velocities. The velocity-porosity trends at the very lowest pressures are shown to be approximately parallel to the sorting trends as represented by the Reuss, Hashin-Shtrikman, and Hardin-Blandford lines. At higher pressures, the velocity increases at a given pressure as a result of compaction are up to 10% greater than the sorting trends for this sample. This behavior is typical for the sand samples, whereas the glass-bead samples tend to show the opposite effect (see Figure 2); the velocity even decreases with compaction at the higher pressures in some of the samples. Inspection of the glass beads after the completion of an experiment does not reveal any damaged grains. The same trend is also apparent in the bulk and shear moduli, so is not just a result of increasing density with compaction. Nevertheless, the total effect of the compaction on the velocities in either the sand or glass-bead samples is relatively small, not exceeding a 10% change from the velocity measured on the initial loading path.

Effect of porosity on the velocity-pressure relationship

To demonstrate the influence of the porosity on the velocity-pressure relationship, a simplified form of Hardin and Blandford's (1989) empirical equations (equation 1) was fitted to the modulus data from each sample. The relationships were modified from those proposed by Hardin and Blandford so that they would be independent of the porosity and could be applied to the water-saturated bulk and constrained moduli:

$$M = M_0 + \mathrm{OCR}^k S p_a^{1-n} p'^n. \tag{6}$$

Here M is the modulus being fit, OCR is the overconsolidation ratio, p' is the effective pressure, p_a is the atmospheric pressure, and S, n, k, and M_0 are treated as free parameters. M_0 is assumed to be zero for the shear modulus and for the dry compressional and constrained moduli. The fit of this expression to the moduli data from sample SC 35% small is shown in Figure 6. This figure demonstrates that both the overall velocity-pressure trend and the effect of compaction on the velocities can be captured effectively by this empirical expression.

Figure 7 shows the fit coefficients for each of the samples plotted against their initial porosities; error bars represent 95% confidence intervals. The lines in each frame of the figure connect the coefficients for the bulk moduli of the same sets of samples as are linked in

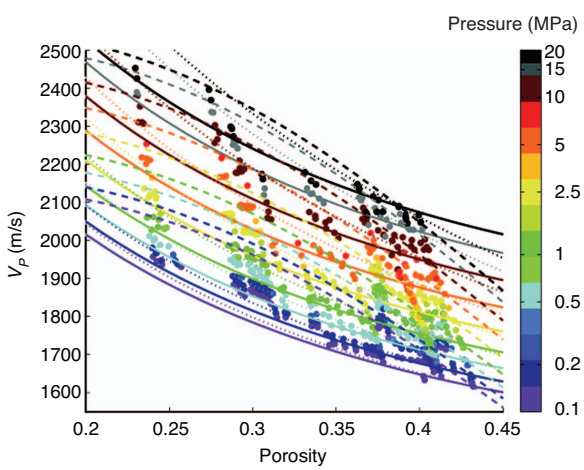

Figure 4. Gassmann fluid-substituted compressional-wave velocities plotted against the porosity and color-coded by pressure. The modified Reuss average (solid), modified Hashin-Shtrikman average (dotted), and Hardin and Blandford empirical (dashed) porosity trends are also shown.

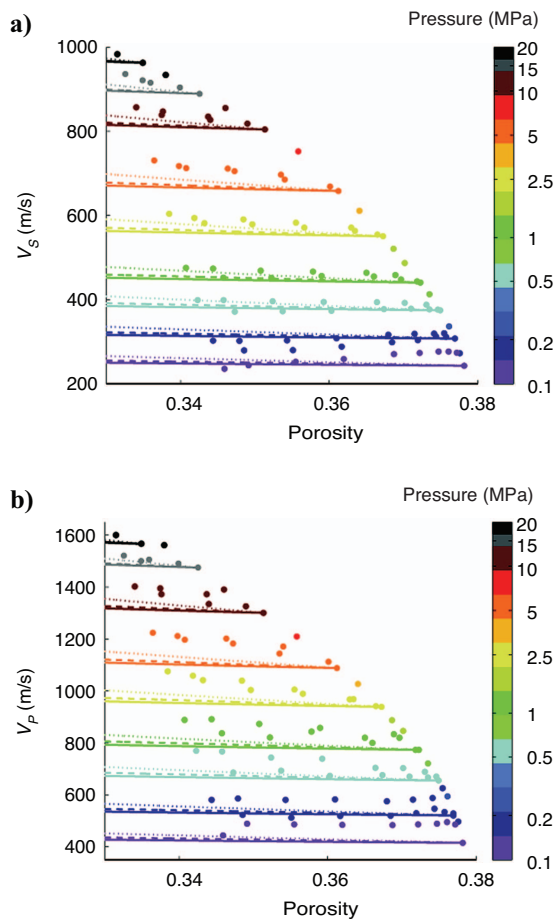

Figure 5. Velocity data from sample SC 35% small. (a) Shear-wave and (b) compressional-wave velocity data plotted against porosity and color-coded by effective pressure. The modified Reuss average (solid), modified Hashin-Shtrikman average (dotted), and Hardin and Blandford empirical (dashed) porosity trends are also shown. These data are represented by the open triangles in Figure 2.

Figure 2; samples SC Big and SC 35% Small are linked by the dotted line, samples GB big, GB 35% small, and GB small are linked by the dashed line, and samples GB big, GB 35% tiny 1, and GB tiny are linked by the solid line. This figure illustrates that for the data set as a whole and for each of these smaller sets of samples, the values of the n, k, and S coefficients for each of the moduli demonstrate no systematic trend relative to the initial porosity. This finding implies that, over this porosity range, the sorting-induced porosity variation does not have a significant impact on the velocity-pressure relationship in unconsolidated sands. The n, k, and S coefficients each demonstrate a considerable amount of nonsystematic variability, which may result from differences in packing produced as the samples were reconstituted or from textural factors other than the sorting. The relatively limited number of samples in this data set and the significant sample-to-sample variation might conceal a weak trend in the fit coefficients that does not meet significance tests ($\chi^2 > 0.05$) for this data set. A more expansive data set with multiple samples for each particle-size distribution and more samples at different porosities would be required to establish statistical significance for what would be at most a weak trend amid the inevitable scatter in data from reconstituted samples. A continuation of this data set to lower porosities might also demonstrate a significant porosity dependence for both the velocities and the velocity-pressure trend coefficients. The velocities of the zero-porosity end member — the pure mineral — are much larger than those observed in our high-porosity samples and demonstrate a much smaller pressure dependence.

Although the change in velocity with pressure, as represented by the n, k, and S coefficients, is mostly independent of the porosity, the values of the moduli at zero pressure (M_0 and K_0) for the fluid-substituted data show a strong, systematic relationship to the porosity. The large porosity dependence of the water-saturated, compressional-wave velocities (see Figure 4) is largely contained in the zero-pressure modulus. The trend of M_0 and K_0 is well described by the Reuss average between water and quartz (shown by the black line in Figure 7f) because when the dry bulk modulus is close to zero, as expected for the zero-pressure condition represented by M_0 and K_0, the Gassmann prediction will be approximately equal to this Reuss average. This similarity of the Gassmann prediction to the Reuss average at low pressure suggests that an approximate porosity correction based on this simple Reuss average could be applied to the water-saturated bulk and constrained moduli of unconsolidated sands, even at higher pressures.

DISCUSSION

The Reuss and the Hashin-Shtrikman lower bounds express the minimum moduli possible for mixtures of two homogeneous materials. Here we use modified forms of these bounds to estimate the moduli of a mixture of a high-porosity framework at a given pressure and of the pure mineral that makes up the grains. These averages represent the effect of replacing a fraction of the high-porosity framework with solid mineral. This substitution is analogous to replacing the equivalent pore volume of that fraction with the mineral, if no change in the rest of the dry frame is assumed. For this data set, the pore filling consists of adding smaller grains to a well-sorted, high-porosity, granular material. The ability of these modified bounds to describe the velocity-porosity trends implies that the porosity reduction resulting from the addition of these smaller grains produces the minimum stiffening theoretically possible. The smaller grains do not sit completely passively in the pore space, but contribute only slightly to the stiffness of the grain framework. The variability in the measurements, especially the fact that some of the measurements plot below the modified Reuss average, indicates that the samples are not exactly represented by a mixture of quartz and the framework that makes up the highest-porosity sample. This finding is to be expected, given that the individually reconstituted samples would not perfectly replicate the framework of that high-porosity sample. These observations corroborate those of Blangy et al. (1993), Dvorkin and Nur (1996), and Avseth et al. (2000), who found modified forms of the Reuss bound or the lower Hashin-Shtrikman bound to effectively describe the velocity-porosity trends of similarly textured, undisturbed sands.

Over the porosity range of the samples prepared for this study, 0.26–0.44, these trends suggest an especially weak sorting-related velocity-porosity trend at low pressures. At pressures below 1 MPa, the large-grain-size sample of each set of bimodal mixtures demonstrates the largest velocities of the set (lines in Figure 2). This result suggests that at these pressures, the variability in the velocities at a given pressure may not be entirely random scatter caused by sample reconstitution but may be systematically related to other textural factors such as the grain size or grain shape. At pressures above 1 MPa, the fact that the mixed-grain-size samples of each set demonstrate the highest velocities suggests that at these pressures, the porosity-related variation exceeds the effects of the other textural differences, possibly because of larger porosity effects as well as diminishing impacts of the grain size, grain shape, and packing at higher pressures.

In the dry samples, the effect on the velocities of porosity variation from 0.26 to 0.44 is much smaller than the effect of the pressure change from 0.1 to 20 MPa (Figure 8a). In the water-saturated case, the porosity effects are larger at low pressure and more consistent at all pressures, whereas the pressure effects are 50% smaller than for the dry case. Porosity variation has only a limited impact on pressure predictions generated from either the compressional- or shear-wave velocities in dry or gas-filled sands. However, in unconsolidated, water-saturated sands, the porosity will generate a significant uncertainty in pressure predictions based on the compressional-wave ve-

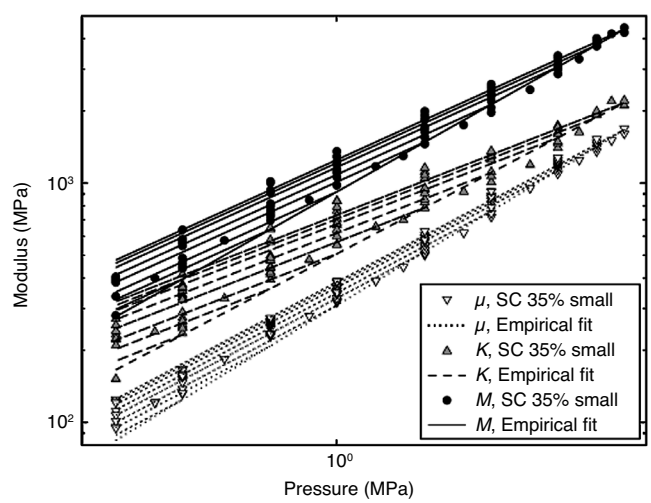

Figure 6. Shear (μ), bulk (K), and P-wave (M) modulus data from sample SC 35% small plotted in a log-log plot against the effective pressure. Lines show the fit of the simplified Hardin-Blandford empirical forms (equation 6) to the data.

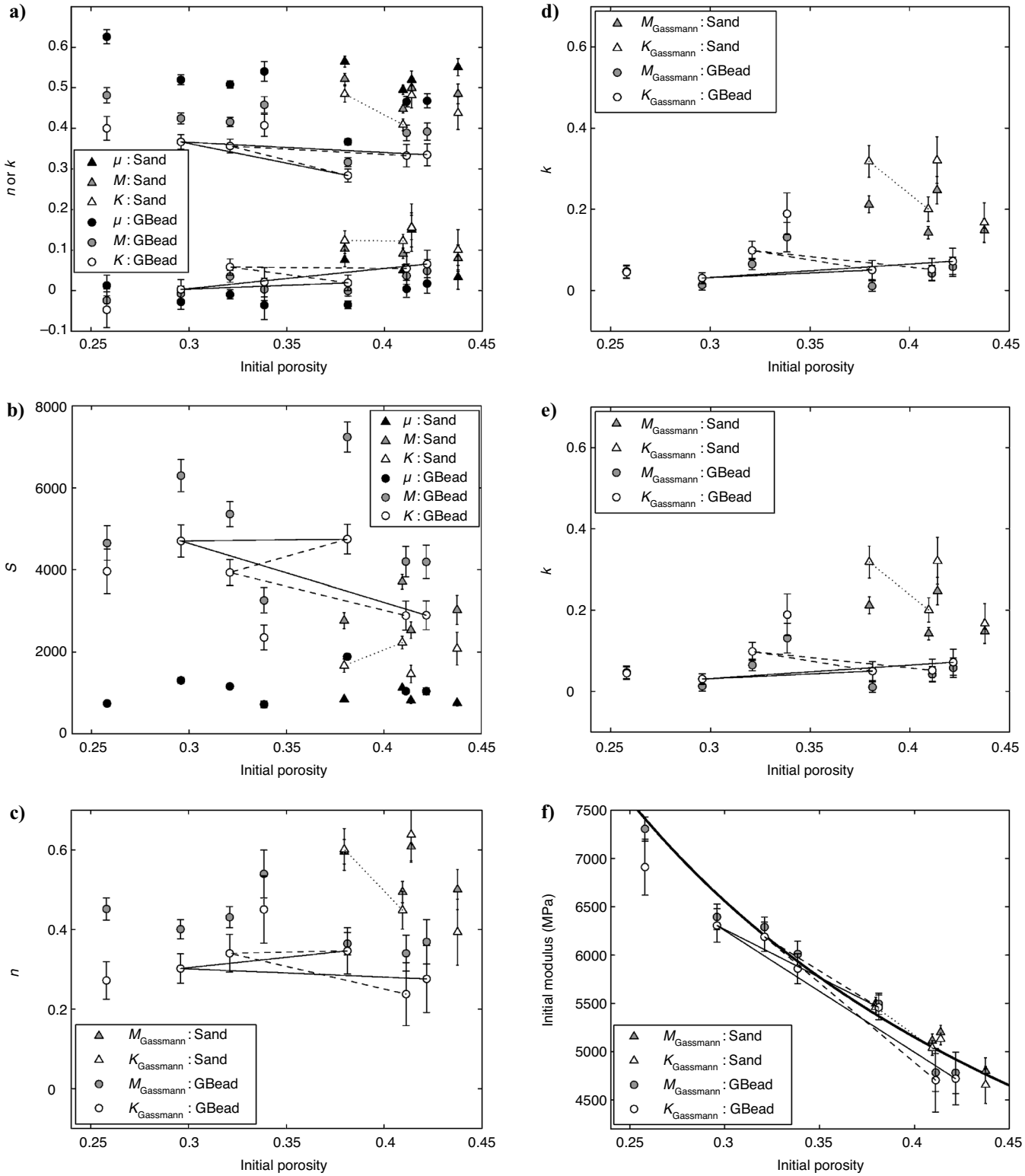

Figure 7. Fit parameters for the moduli (μ, shear modulus; M, P-wave modulus; K, bulk modulus) of each of the samples plotted against the initial porosity of the sample: (a) n and k and (b) S for the dry samples; (c) n, (d) k, (e) S, and (f) K_0 and M_0 for the water-saturated samples. The thick black line in (f) represents the Reuss bound for quartz and water. The thin lines connect the coefficients from sets of samples made up of bimodal mixtures of two grain sizes: dotted line — samples SC big, SC 35% small; dashed line — samples GB big, GB 35% small, GB small; solid line — samples GB big, GB 35% tiny 1, GB tiny.

locities. In this case, accurate pressure prediction requires the use of additional information, such as shear-wave velocities, V_P/V_S ratio measurements, or porosity data.

The shear-wave velocity-porosity trend in water-saturated sands is essentially unchanged from the dry trends, where the porosity effects are small. As up to 200 m/s of variability in the shear-wave velocity remains between the different samples (Figure 8a), there can be significant uncertainty in pressures predicted from the shear-wave velocities unless empirical velocity-pressure relationships are calibrated to the specific sediment of interest.

Although the V_P/V_S ratio calculated from the velocities of the dry samples is essentially constant with pressure (Figure 8b), in the water-saturated case, the V_P/V_S ratio is highly sensitive to pressure (Huffman and Castagna, 2001; Prasad, 2002). However, at pressures below 2 MPa, the water-saturated V_P/V_S ratio varies by more than 50%. At low pressures, the shear-wave velocities do not show a significant porosity dependence but appear to be sensitive to other textural factors. The shear-wave velocities therefore do not cancel the systematic porosity variation in the water-saturated compressional-wave velocities. As most of the variability in the shear-wave velocities at low pressure is not correlated to the porosity, a simple porosity correction does not reduce the uncertainty in pressure predictions based on V_P/V_S ratio measurements. At higher pressures, the porosity trend of the shear-wave velocities, while small in absolute terms, is of approximately the same relative magnitude as that of the water-saturated compressional-wave velocities. For this reason, and because the larger shear-wave velocities at higher pressures do not produce as much variability in the V_P/V_S ratio for the same variation in velocity, we see less scatter in the V_P/V_S ratio above ~ 5 MPa.

Porosity correction of pressure predictions from the compressional-wave velocities can be performed by using Gassmann's equation to calculate the dry compressional-wave velocity, which could then be used to predict the pressure directly. Alternatively, the dry velocities could also then be corrected for porosity by using the modified Reuss or Hashin-Shtrikman trends and then be transformed back to the water-saturated state at some desired reference porosity. This transformation using Gassmann's equations also requires knowledge of the shear-wave velocities and is sensitive to uncertainties in the porosity and density.

A second approach to correcting for the porosity effects on pressure predictions from the water-saturated compressional-wave velocities is based on the Reuss bound of the constrained modulus. On the basis of the assumption that the velocity-pressure relationship, represented by the empirical coefficients n, k, and S in equation 6, is independent of porosity, the water-saturated compressional-wave velocity needs only to be corrected for the porosity dependence of the zero-pressure modulus M_0. In unconsolidated sands where the shear modulus can be assumed to be zero at zero pressure, M_0 and K_0 — the constrained and bulk moduli of water-saturated sediments at zero pressure, respectively — are equal. By assuming that the dry bulk modulus is much smaller than the bulk modulus of the pure mineral, a safe assumption at low pressure in unconsolidated sands, Gassmann's equation reduces to the Reuss bound. The water-saturated zero-pressure constrained modulus M_0 at a given porosity can therefore be predicted from the Reuss bound. The correction is then performed by adding the difference between the Reuss bound value at any desired reference porosity, $M_{\mathrm{Reuss},\phi_R}$, and that at the porosity of the sediment, M_{Reuss}, to the empirical coefficient for the constrained modulus, M_0:

$$M_{0,\phi_R} \approx (M_{\mathrm{Reuss},\phi_R} - M_{\mathrm{Reuss}}) + M_0. \tag{7}$$

This correction is an approximate form of the Gassmann-based correction described in the previous paragraph, except that equation 7 neglects any porosity dependence not contained in the zero-pressure modulus. The velocity calculation also requires that the density be corrected to the reference porosity according to the following:

$$\rho_{\mathrm{sat},\phi_R} = (1 - \phi_R)\rho_{\mathrm{min}} + \phi_R \rho_{fl}, \tag{8}$$

where $\rho_{\mathrm{sat},\phi_R}$ is the corrected density, ρ_{min} is the pure-mineral density, assumed to be that of quartz (2650 kg/m^3), and ρ_{fl} is the density of the saturating fluid. Comparisons of the original water-saturated compressional-wave velocities to those corrected for the porosity effects by using equations 7 and 8 are shown in Figure 9. The correction collapses the variation in the water-saturated compressional-wave velocity by 50% at the highest pressures, but is more effective at reducing the scatter at the lower pressures. The remaining variation results from random variations caused by sample reconstitution from other textural factors besides the porosity, and from any sys-

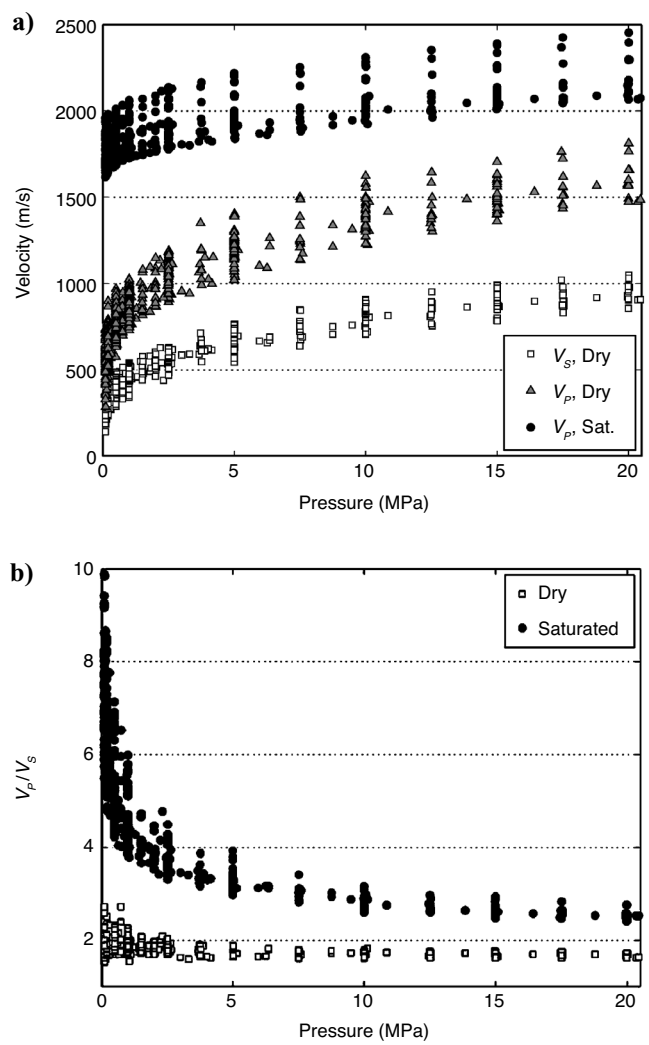

Figure 8. (a) Velocity and (b) V_P/V_S ratio data from all of the samples plotted against the effective pressure.

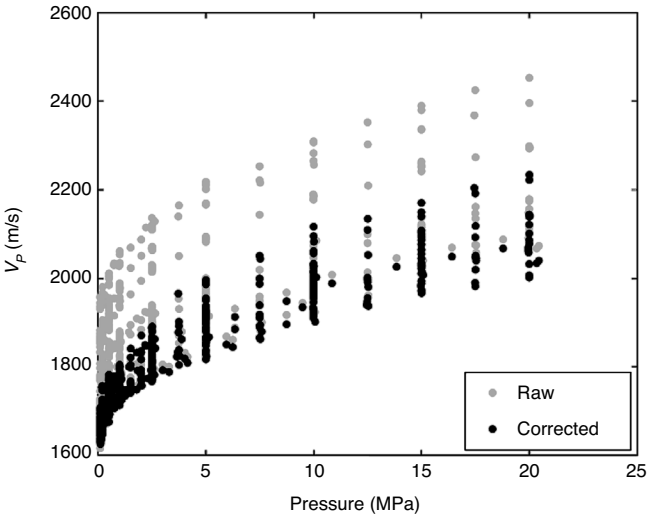

Figure 9. Comparison of raw and porosity-corrected, water-saturated compressional-wave velocities, plotted against effective pressure. The velocity values were all corrected to a reference porosity of 0.4 by using equations 7 and 8.

tematic, porosity-related variation not contained in the zero-pressure bulk modulus.

CONCLUSIONS

To isolate the impact of sorting- and compaction-related porosity variation on the seismic velocities and their pressure dependences, we measured the velocities and porosity of a set of similarly prepared synthetic sand and glass-bead samples, mostly with bimodal grain-size distributions. These measurements demonstrate that the sorting-related porosity decrease produces less than a 10% increase in the shear-wave velocities and less than a 15% increase in the compressional-wave velocities of unconsolidated, noncohesive, dry sediments at pressures of up to 20 MPa. On the contrary, for water-saturated velocities modeled with Gassmann fluid substitution, the measurements show, as expected, a significant, systematic increase in the compressional-wave velocity with decreasing porosity. The substitution of water for air in the pores produces a greater stiffening of the lower-porosity sediments, resulting in consistently higher velocities at lower porosities. The velocity-porosity trends for both the dry and water-saturated cases are well described by the Reuss average between the moduli of the highest-porosity sample at a given pressure and the moduli of quartz.

Porosity reduction from compaction results in velocity increases of up to 10% at a given pressure for individual sand samples. This effect is very similar to the sorting effect at lower pressures, but exceeds the sorting effect for the same change in porosity at high pressures.

Over the porosity range of our samples, the sorting demonstrates no significant, systematic effect on the velocity-pressure relationship of the shear, bulk, or constrained moduli, as described by the fit coefficients to simplified Hardin and Blandford equations. The nonsystematic scatter of these pressure dependences with the initial porosity of the samples is larger than any apparent sorting effect. For the water-saturated moduli modeled with Gassmann fluid substitution, a significant porosity dependence is evident in the empirical coefficient representing the zero-pressure modulus of the bulk and constrained moduli (M_0 and K_0).

Because many other factors besides sorting and compaction can influence the velocity-porosity relationship, including variations in texture, fluid content, or diagenetic history, the relationships between the porosity, pressure, and velocity in natural sediments could differ from the trends presented here. Nevertheless, we expect the qualitative patterns observed here to be valid for measurements made in situ and for laboratory measurements on undisturbed, natural sands. Specifically, the limited effect of the porosity variations attributable to sorting on the dry velocities and their pressure dependences and the large porosity effects observed in the water-saturated compressional-wave velocities should hold in natural sands.

ACKNOWLEDGMENTS

Funding for this work was provided by the Stanford Rock Physics and Borehole Geophysics Consortium, by a Chevron Stanford Graduate Fellowship (to Zimmer), and by the U. S. Department of Energy under grants DE-FG03-99ER14933 and DE-FC2601BC15354. The opinions, findings, conclusions, and recommendations expressed herein are those of the authors and do not necessarily reflect the views of the DOE. We appreciate the assistance of Gilbert Palafox in the construction of the experimental apparatus.

REFERENCES

Avseth, P., J. Dvorkin, G. Mavko, and J. Rykkje, 2000, Rock physics diagnostic of North Sea sands: Link between microstructure and seismic properties: Geophysical Research Letters, **27**, 2761–2764.

Beard, D. C., and P. K. Weyl, 1973, Influence of texture on porosity and permeability of unconsolidated sand: AAPG Bulletin, **57**, 349–369.

Blangy, J. P., S. Strandenest, D. Moos, and A. Nur, 1993, Ultrasonic velocities in sands — Revisited: Geophysics, **58**, 344–356.

Cumberland, D. J., and R. J. Crawford, 1987, The packing of particles: Elsevier Science Publ. Co., Inc..

Dvorkin, J., and A. Nur, 1996, Elasticity of high porosity sandstones: Theory for two North Sea data sets: Geophysics, **61**, 1363–1370.

Eberhart-Phillips, D., D.-H. Han, and M. D. Zoback, 1989, Empirical relationships among seismic velocity, effective pressure, porosity, and clay content in sandstone: Geophysics, **54**, 82–89.

Freund, D., 1992, Ultrasonic compressional and shear velocities in dry clastic rocks as a function of porosity, clay content, and confining pressure: Geophysical Journal International, **108**, 125–135.

Han, D.-H., A. Nur, and D. Morgan, 1986, The effects of porosity and clay content on wave velocities in sandstones: Geophysics, **51**, 2093–2107.

Hardin, B. O., and G. E. Blandford, 1989, Elasticity of particulate materials: Journal of Geotechnical Engineering, **115**, 788–805.

Hardin, B. O., and V. P. Drnevich, 1972, Shear modulus and damping in soils: Design equations and curves: Journal of the Soil Mechanics and Foundations Division, American Society of Civil Engineers, **98**, 667–692.

Hashin, Z., and S. Shtrikman, 1963, A variational approach to the elastic behavior of multiphase materials: Journal of the Mechanics and Physics of Solids, **11**, 127–140.

Huffman, A. R., and J. P. Castagna, 2001, The petrophysical basis for shallow-water flow prediction using multicomponent seismic data: The Leading Edge, **20**, 1030–1052.

Jones, S. M., 1995, Velocities and quality factors of sedimentary rocks at low and high effective pressures: Geophysical Journal International, **123**, 774–780.

Khaksar, A., C. M. Griffiths, and C. McCann, 1999, Compressional- and shear-wave velocities as a function of confining stress in dry sandstones: Geophysical Prospecting, **47**, 487–508.

Mavko, G., T. Mukerji, and J. Dvorkin, 1998, The rock physics handbook: Tools for seismic analysis in porous media: Cambridge University Press.

Nur, A., G. Mavko, J. Dvorkin, and D. Gal, 1995, Critical porosity: The key to relating physical properties to porosity in rocks: 65th Annual International Meeting, SEG, Expanded Abstracts, 878.

Prasad, M., 2002, Acoustic measurements in sands at low effective pressure and overpressure detection: Geophysics, **67**, 405–412.
Walton, K., 1987, The effective elastic moduli of a random packing of spheres: Journal of the Mechanics and Physics of Solids, **35**, 213–226.
Wyllie, M. R. J., A. R. Gregory, and G. H. F. Gardner, 1958, An experimental investigation of factors affecting elastic wave velocities in porous media: Geophysics, **23**, 459–493.
Zimmer, M. A., 2003, Seismic velocities in unconsolidated sands: Measurements of pressure, sorting, and compaction effects. Ph.D. thesis, Stanford University.
Zimmer, M. A., M. Prasad, G. Mavko, and A. Nur, 2007, Seismic velocities of unconsolidated sands: Part 1. Pressure trends from 0.1 to 20 MPa: Geophysics, this issue.